Research in Astronomy and Astrophysics, 25:035003 (6pp), 2025 March
https://doi.org/10.1088/1674-4527/adb36d
CSTR: 32081.14.RAA.adb36d

Examination of Radiative Capture Rates of ^{99}Tc(n, γ)^{100}Tc and Stellar β^- Decay Rates of ^{99}Tc

Abdul Kabir[1], Jameel-Un Nabi[2], Muhammad Tahir[2], Zain Ul Abideen[1], and Isha Mudassir[1]
[1] Space and Astrophysics Research Lab, National Centre of GIS and Space Applications, Department of Space Science, Institute of Space Technology, Islamabad, 44000, Pakistan; kabirkhanak1@gmail.com
[2] University of Wah, Quaid Avenue, Wah Cantt 47040, Punjab, Pakistan
Received 2024 December 6; revised 2025 January 17; accepted 2025 February 2; published 2025 February 28

Abstract

Within the context of the proton–neutron quasi-particle random phase approximation (pn-QRPA) model and TALYS v1.96 code, the radiative capture (^{99}Tc$(n,\gamma)^{100}$Tc) and stellar weak interaction ($^{99}\text{Tc} \rightarrow {}^{99}\text{Ru} + e^- + \nu_e$) rates were computed during thermal pulses operating in asymptotic giant branch stars. The Maxwellian average cross-section (MACS) and neutron capture rates for the ^{99}Tc$(n,\gamma)^{100}$Tc process are analyzed within the context of statistical code TALYS v1.96. The effect of nuclear level density (NLD) and γ-strength functions on MACS and neutron capture rates has been examined. The model-based computations for MACS provided an insightful contrast to prior investigated findings. The sensitivity of stellar weak interaction rates to different densities and temperatures is investigated using the pn-QRPA model. The impact of thermally populated excited states on electron emission (β^-) rates in ^{99}Tc is extensively examined. Additionally, a comparison is made between the study of the stellar β^-decay rates and the thermal neutron capture rates. It is found that at $T_9 = 0.26$ the thermal neutron capture rates ($\lambda_{(n,\gamma)}$) and the temperature dependent stellar β^-decay rates (λ_{β^-}) cross each other. However, at higher temperatures, the $\lambda_{(n,\gamma)}$ are found to be higher than λ_{β^-}.

Key words: astroparticle physics – nuclear reactions, nucleosynthesis, abundances – stars: AGB and post-AGB – stars: evolution

1. Introduction

Energy production in stars (Bethe 1939), related nucleosynthesis (Burbidge et al. 1957), and supernova explosion dynamics (Baade & Zwicky 1934) are still unclear. The neutron capture process is significant in the quest for matter synthesis in the universe. Similarly, weak interaction-mediated rates dictate the terms and conditions for the process of nucleosynthesis and the dynamics of supernova explosions. Other factors, e.g., magnetorotational effects (Usman & Mushtaq 2023), may also contribute to the instability of a stellar core. Elements more massive than iron are formed by (n,γ) or via the weak interaction processes. The neutron density and temperature of an astrophysical site can be constrained by evaluating the observed abundance distribution of elements with nucleosynthesis predictions utilizing (n,γ) cross-sections and β decay properties.

On the asymptotic giant branch (AGB), S stars are late-type giants that stand in between M-type stars and carbon stars. They are divided into two categories based on the presence of technetium (Tc), i.e., intrinsic and extrinsic. The intrinsic or Tc-rich S stars are thermally pulsing AGB stars that produce *s*-process elements (including Tc) internally. The third dredge-up (TDU) brings these elements to the surface. The Tc-poor or extrinsic S stars obtained their *s*-process abundances through the accretion of *s*-process-rich material from an AGB partner that has subsequently converted into a dim white dwarf (Shetye et al. 2021). Tc is predicted to be generally the unstable neutron capture product. ^{99}Tc isotope produced by the *s*-process has a half-life $T_{1/2}$ of 2.1×10^5 yr. Its detection indicates that this element is currently synthesized by a star located on the AGB. For further investigation one can see Shetye et al. (2020) and references therein. The β-decay lifetime of ^{99}Tc is highly temperature-sensitive (Cameron 1959). The identification of a considerable Tc abundance would then appear to imply that the measured abundances are dominated by products from a slow neutron capture (*s*-process) scenario, and that the developing of Tc might have happened at relatively low *s*-process temperatures of around $T_9 = 0.1$ (Iben & Truran 1978). In the present nucleosynthesis model, the *s*-process is marginally more complex than predicted in Lugaro et al. (2003). From a simple overview of the solar system's elemental abundance pattern, the *s*-process expanded into a more thorough description that incorporates the basic characteristics of stellar and galactic dynamics. These developments have made the *s*-process a successful tool to investigate the formation and evolution of red giant stars (Busso et al. 2001). The β decay lifetime of ^{99}Tc is temperature-sensitive; one should also take into account the fact that the production and destruction of ^{99}Tc depend on the

^{22}Ne$(\alpha, n)^{25}$ Mg reaction rate. The competition between ^{99}Tc$(n, \gamma)^{100}$Tc and ^{99}Tc $\rightarrow$ ^{99}Ru $+ e + \nu_e$ determines the reduction of ^{99}Tc in the *s*-process environment. Therefore, higher temperatures do not always result in lower Tc abundances. The increased neutron production from the ^{22}Ne$(\alpha, n)^{25}$ Mg reaction at high temperatures more than compensates for the thermally enhanced β-decay rate (Mathews et al. 1986).

We draw the reader's focus toward the competition between ^{99}Tc$(n, \gamma)^{100}$Tc and ^{99}Tc $\rightarrow$ ^{99}Ru $+ e + \nu_e$ processes within the context of statistical code and proton–neutron quasi-particle random phase approximation (pn-QRPA) model. The Tc abundance measures the lifetime of the TDU phase for AGB stars. The Maxwellian average cross-section (MACS) of ^{99}Tc is a crucial input parameter in determining τ_d. The ^{99}Tc(n, γ) has a relatively large cross-section of the reaction, making ^{99}Tc a potential candidate for transmutation using neutrons. Macklin (1982) analyzed the cross-section of reaction ^{99}Tc(n, γ) within (2.65–2000) keV with an uncertainty of (4.0–4.9)%. Their obtained average cross-section is in agreement with the ENDF/$B-V$ evaluation for energies above 900 keV and falls within the $\pm$15% range relative to the JENDL-1 evaluation for energies below 700 keV. Harada et al. (1995) measured the resonance integral of ^{99}Tc$(n, \gamma)^{100}$Tc and thermal neutron capture cross-section by employing the activation method. The measured values for the thermal neutron capture cross-section and the resonance integral were 22.9 $\pm$ 1.3 b and 398 $\pm$ 38 b, respectively.

^{99}Tc in the present work is a stable isotope ($T_{1/2} =$ 211,100 yr) of Tc in the terrestrial environment. However, considering the age of a low mass star, it is not a stable isotope. The parent nuclei's excited states have a significant occupancy probability because of the extreme temperature (10^9 K) conditions found in stellar matter. As a consequence, the total stellar weak rates have visible contributions from each excited state (Bisterzo et al. 2015). As such, the microscopic rate-calculating approach has to incorporate all partial decay rates owing to distinct parent excited states. The pn-QRPA model (Klapdor-Kleingrothaus et al. 1984) is based on a state-by-state examination of weak interaction-mediated rates. The pn-QRPA approach was utilized for the first time to determine microscopic weak interaction rates for a large number of accessible nuclei far from the stability line. The pn-QRPA approach has been developed using multiple forms of potential and the mean-field basis, for example, the deformed Nilsson model (Hirsch et al. 1992), the FRDM with a folded Yukawa single-particle potential (Möller & Randrup 1990), and the Woods–Saxon potential (Hektor et al. 2000).

In the present investigation, we have computed the MACS for the (n, γ) in the framework of TALYS v1.96. Based on the best-fitted model, we have calculated the $\lambda_{(n,\gamma)}$ for ^{99}Tc $+ n \rightarrow$ ^{100}Tc $+ \gamma$. As we previously discussed, the temperature conditions in the stellar matter are so extreme (10^9 K) that there is a substantial possibility of the parent nuclei's excited states being occupied. As a consequence, the total stellar weak rates are discernible contributions from each particular excited state. Hence, we utilized the pn-QRPA approach to analyze the stellar weak rates.

The current study is organized as follows: Section 2 gives a brief review of the underlying formalism. Section 3 outlines our calculations and compares them to past calculations and experiments. Our outcomes are laid out in Section 4.

2. Formalism

2.1. The Statistical Model

The (n, γ) process for the heavy mass nuclei was analyzed within the context of TALYS (Kabir et al. 2024). The Hauser–Feshbach (H-B) theory (Hauser & Feshbach 1952) serves as the foundation for the TALYS v1.96 code. There are three primary inputs for the H-B theory, including the γ- strength functions, optical potentials, and nuclear level densities (NLDs). In the present study, the local OP (Koning & Delaroche 2003) is utilized. The outcomes were examined using the back-shifted Fermi gas model (BSFM) (Dilg et al. 1973) for the NLD, and similarly, the Gogny D1M HFB+QRPA (Goriely et al. 2018), Brink–Axel Lorentzian (Brink 1957), and Kopecky–Uhl Lorentzian (Kopecky & Ulh 1990) for the γ-strength functions. The MACS is calculated using neutron energy of up to 100 keV. The MACS is described here

$$\langle \sigma \rangle = \frac{2}{\sqrt{\pi}(k_B T_9)^2} \int_0^\infty E_{cm}\sigma(E_{cm}) \exp\left(\frac{-E_{cm}}{k_B T_9}\right) dE. \quad (1)$$

T_9 is the core temperature ($T_9 = 10^9$ K), $\sigma(E_{cm})$ is the capture cross-section in the center of mass system, k_B is the Boltzmann constant, and E_{cm} is the projectile energy in the center of mass system. Level densities at excitation energies (E_x) when experimental data are unavailable must be derived from theoretical predictions. Here, we employed the statistical models for predicting nuclear processes. A comprehensive theoretical examination of angle distributions, cross-sections, and other nuclear attributes desires an exact level density (LD) in addition to the optical model potential. In the current investigation, the BSFM was utilized for NLD. By considering pairing energy as a dynamic parameter, the BSFM functions cover a wide range of energy levels. It is explained below

$$\rho_F^{tot}(E_x) = \frac{1}{\sqrt{2\pi}\sigma} \frac{\sqrt{\pi}}{12} \frac{\exp(2\sqrt{aU})}{a^{1/4}U^{5/4}}, \quad (2)$$

where U represents the effective energy, σ represents the spin cut-off, and a indicates the adaptable variable given below.

$$a = \left(1 + \delta W \frac{1 - \exp(-\gamma U)}{U}\right) \times \tilde{a}$$
$$\text{where} \quad \tilde{a} = \alpha A + \beta A^{2/3}, \quad (3)$$

where α, β, and γ are global parameters that must be taken into account in order to provide the best average LD approximation throughout the whole spectrum of nuclides. A denotes the mass number and $\tilde{a}$ is the asymptotic LD. The shell correction energy is δW, and the rate at which a approaches $\tilde{a}$ is determined by the damping parameter γ. The LD parameter a can be adjusted for optimal alignment and suitable nuclear implications. For further insight into the formalism, one can refer to Koning et al. (2008). TALYS v1.96 employs different γ-strength functions, incorporating the Brink–Axel model for all transitions with the exception of $E1$ (Koning et al. 2021). The distribution of average reduced partial transition width as a function of photon energy E_γ is given by the γ-strength function $f_{\rm XL}$ for Brink–Axel.

$$f_{\rm XL}(E_\gamma) = K_{\rm XL}\frac{\sigma_{\rm XL}E_\gamma\Gamma_{\rm XL}^2}{(E_\gamma^2 - E_{\rm XL}^2)^2 + (E_\gamma\Gamma_{\rm XL})^2}, \quad (4)$$

where $E_{\rm XL}$ is the energy, $\Gamma_{\rm XL}$ is the width and $\sigma_{\rm XL}$ is the resonant strength. The Kopecky–Uhl model is used by default for the analysis of $E1$ transitions.

$$f_{\rm XL}(E_\gamma, T) = K_{\rm XL}\left[\frac{E_\gamma\tilde{\Gamma}_{E1}(E_\gamma)}{(E_\gamma^2 - E_{E1}^2)^2 + E_\gamma^2\tilde{\Gamma}_{E1}(E_\gamma)^2} + \frac{0.7\Gamma_{E1}4\pi^2T^2}{E_{E1}^5}\right]\sigma_{E1}\Gamma_{E1}, \quad (5)$$

and

$$\tilde{\Gamma}_{E1}(E_\gamma) = \Gamma_{E1}\frac{E_\gamma^2 + 4\pi^2\left[\frac{E_n + S_n - \Delta - E_\gamma}{a(S_n)}\right]}{E_{E1}^2}, \quad (6)$$

where $\tilde{\Gamma}(E_\gamma)$ and E_n represent the damping width and neutron energy respectively. Δ is the pairing correction, and S_n is the separation energy for a single neutron. Large-scale computations of the $E1$ and $M1$ absorption γ-ray strength function are performed using the Gogny-HFB+QRPA dipole strength function in the context of the axially symmetric deformed quasi-particle random phase approximation (QRPA). This depends on the finite range D1M Gogny force to describe the de-excitation strength function. The low-energy contributions (D1M+QRPA+0lim) are included in the total $M1$ and $E1$ strengths, and are distributed as follows:

$$f_{E1}(\varepsilon_\gamma) = f_{E1}^{\rm QRPA}(\varepsilon_\gamma) + f_0\,U/[1 + e^{(\varepsilon_\gamma - \varepsilon_0)}], \quad (7)$$

$$f_{M1}(\varepsilon_\gamma) = f_{M1}^{\rm QRPA}(\varepsilon_\gamma) + C\,e^{-\eta\varepsilon_\gamma}, \quad (8)$$

where U represents the initial de-exciting state's excitation energy. The D1M+QRPA electric or magnetic dipole strength at the photon energy ε_γ is denoted by the expression $f_{X1}^{\rm QRPA}$. η, f_0, ε_0, and C are dynamical parameters.

2.2. The pn-QRPA Model

We investigate the stellar weak rates within the context of pn-QRPA. The model's Hamiltonian is displayed as

$$H^{\rm QRPA} = H^{\rm sp} + V^{\rm pair} + V_{\rm GT}^{\rm ph} + V_{\rm GT}^{\rm pp}. \quad (9)$$

The single-particle energies and the wave functions have been determined utilizing the distorted Nilsson potential ($H^{\rm sp}$) basis. The Bardeen–Cooper–Schrieffer (BCS) formalism was utilized to handle the pairing forces of $V^{\rm pair}$. The $V_{\rm GT}^{\rm ph}$ (χ (ph)) is the particle–hole interaction potential, and $V_{\rm GT}^{\rm pp}$ (κ (pp)) is the particle–particle interaction potential. They are also known as the residual interactions, which are crucial for the analysis of Gamow-Teller (GT) strength. For a detailed explanation of χ and κ, as well as the best way to optimize these values, one can see Staudt et al. (1990).

The $V_{\rm GT}^{\rm ph}$ force was found employing

$$V_{\rm GT}^{\rm ph} = +2\chi\sum_{\mu=-1}^{1}(-1)^\mu Y_\mu Y^\dagger_{-\mu}, \quad (10)$$

with

$$Y_\mu = \sum_{j_pm_pj_nm_n}\langle j_pm_p|t_-\,\sigma_\mu|j_nm_n\rangle c^\dagger_{j_pm_p}c_{j_nm_n}. \quad (11)$$

Whereas the V_{GT}^{pp} interaction was determined employing

$$V_{\rm GT}^{\rm pp} = -2\kappa\sum_{\mu=-1}^{1}(-1)^\mu P_\mu^\dagger P_{-\mu}, \quad (12)$$

with

$$P_\mu^\dagger = \sum_{j_pm_pj_nm_n}\langle j_nm_n|(t_-\sigma_\mu)^\dagger|j_pm_p\rangle \times (-1)^{l_n+j_n-m_n}c^\dagger_{j_pm_p}c^\dagger_{j_n-m_n}, \quad (13)$$

where the operators are explained below and the other symbols have their normal meanings. The χ and κ were taken from Homma et al. (1996). Reduced GT transition probabilities have been obtained by representing the QRPA ground state as one-phonon states in the daughter nucleus. Supplementary input parameters for the investigation of weak transitions encompass the pairing gap (Δ_p, Δ_n), nuclear deformation (β_2), and the critical quantities of energy and Nilsson potential parameters (NPPs). We updated the calculations with nuclear deformation parameters from the most recent investigation (Möller et al. 2016). The NPP was obtained from Ragnarsson & Sheline (1984), and the oscillation constant was calculated utilizing $\hbar\omega = \frac{41}{A^{1/3}}$ (in MeV). We utilized the Nilsson potential with the deformed basis to analyze wave functions. The Nilsson potential is frequently utilized to describe the structure of low-lying states. We also utilized the nuclear deformations as a Nilsson potential input parameter. The deformed Nilsson basis was mainly employed for analyzing wave functions and single-particle energies. The transformation from the spherical

nucleon basis (c^{+}_{jm}, c_{jm}) to the axial symmetric deformed basis ($d^{+}_{m\alpha}$, $d_{m\alpha}$) was performed

$$d^{+}_{m\alpha} = \sum_{j} D^{m\alpha}_{j} c^{+}_{jm}. \quad (14)$$

A set of Nilsson eigenfunctions with α as a supplementary quantum number to describe the Nilsson eigen-states are identified as the $D^{m\alpha}_{j}$. For the nucleonic system including protons and neutrons, the BCS framework is used independently in the Nilsson basis. The transformation matrices were obtained by diagonalizing the Nilsson Hamiltonian (a further description can be found in Hirsch et al. 1993). The globally consistent pairing gap values, $\Delta_n = 12/\sqrt{A}$ (MeV) (for neutrons) and $\Delta_p = 12/\sqrt{A}$ (MeV) (for protons), have been employed in our examination. The Q-value of the reaction was computed to be 0.2975 MeV (Kondev et al. 2020). For further insight into the formalism of Equation (9), one can refer to Muto et al. (1992). The analysis of terrestrial β^{-} half-lives has been shown in Staudt et al. (1990). There are further details available in Nabi & Klapdor-Kleingrothaus (1999) on the formalism used to forecast the GT transitions under stellar conditions utilizing the pn-QRPA approach.

From the parent nucleus to the daughter nucleus, the electron emission rates ($\lambda^{\beta^{-}}_{ij}$) can be obtained by

$$\lambda^{\beta^{-}}_{ij} = \ln 2 \frac{f_{ij}(T, \rho, E_f)}{(ft)_{ij}}, \quad (15)$$

where the reduced transition probability (B_{ij}) is linked to $(ft)_{ij}$ via the

$$(ft)_{ij} = D/B_{ij}. \quad (16)$$

B_{ij} has been explained below, and D is set as 6143 s according to (Hardy & Towner 2009)

$$B_{ij} = B(F)_{ij} + (g_A/g_V)^2 B(GT)_{ij}. \quad (17)$$

The reduced transition probabilities of the Fermi and GT transitions, respectively, are denoted by B(F) and B(GT). The phase space factor, f_{ij}, is extensively described in Nabi & Klapdor-Kleingrothaus (2004). The β^{-} decay rates are mostly sensitive to parent excited energy levels because of the high temperatures in the stellar core. The parent nucleus' occupancy probability is obtained utilizing the Boltzmann distribution.

$$P_i = \frac{\exp(-E_i/kT)}{\sum_{i=1} \exp(-E_i/kT)}. \quad (18)$$

Additionally, the total stellar β^{-} rates have been analyzed using

$$\lambda^{\beta^{-}} = \sum_{ij} P_i \lambda^{\beta^{-}}_{ij}. \quad (19)$$

The summation over parent and daughter states was carried out until a desired convergence level was achieved in our rate calculation. We employed a large model space (7 $\hbar\omega$) for weak β^{-} analysis. The necessary convergence is facilitated by the large model space. One of the key benefits of the pn-QRPA approach is its ability to compute the weak β^{-} rates for any nuclear species with $A > 20$.

2.3. The Stellar Neutron Capture Rates ($\lambda_{(n,\gamma)}$)

According to Mathews et al. (1986), the $\lambda_{(n,\gamma)}$ for $^{99}\mathrm{Tc} + n \rightarrow {}^{100}\mathrm{Tc} + \gamma$ is determined as

$$\lambda_{(n,\gamma)} = 2.0 \times 10^{-16} n_n \ \mathrm{s}^{-1}. \quad (20)$$

n_n represents neutron density at $T_9 < 1$, which is further defined below

$$n_n = \frac{4.3 \times 10^{36} \rho X_4 e^{[-(0.197/T_9)^{4.82}]} \left(\frac{1}{T_9}\right)^{2/3} e^{\frac{-47}{(T_9)^{1/3}}}}{\sigma_{22}[1 + \sigma_i N_i / \Sigma \sigma_{22} N_{22}] \left(\frac{T_9}{0.348}\right)^{1/2}} \ \mathrm{cm}^{-3}. \quad (21)$$

X_4, ρ and T_9 are the helium mass fraction, nuclear matter density, and stellar temperature, respectively. σ_{22} represents the capture cross-section for $^{22}\mathrm{Ne}(n,\gamma)^{23}\mathrm{Ne}$. N_i represents the abundance of species i, whereas σ_i denotes their Maxwellian average neutron capture cross-section. Heavy nuclei at the base of the convective shell are dominated by ^{22}Ne formed by α-captures on ^{14}N from the CNO cycle.

3. Results and Discussion

For specific applications, such as astrophysical investigations involving nuclei along neutron or proton drip lines, the data must be predicted well beyond the experimentally known region. As a result, data from reliable theoretical models need to be employed in large-scale applications. It has been found that incorrect NLD description or prediction causes the most uncertainty in statistical model computations. Theoretical extrapolations are required since experiments are not feasible at all energies. We computed the MACS for ^{99}Tc by utilizing the NLDs and γ-strength functions. We have investigated the MACS of the $^{99}\mathrm{Tc}(n,\gamma)^{100}\mathrm{Tc}$ reaction for a range of temperatures appropriate for the presumed site of the s-process. Using TALYS in the H-B framework, the MACS of the $^{99}\mathrm{Tc}(n,\gamma)^{100}\mathrm{Tc}$ reaction was calculated by selecting a radiative strength function and the NLD. We used phenomenological NLDs as BSFM for excitation energies up to 100 keV. In the present analysis, the BSFM is adjusted for NLD and the Gogny, Kopecky–Uhl, and Brink–Axel models for the γ-strength function.

The analysis of the MACS for ^{99}Tc within ($0.01 < kT < 100$) keV which is appropriate for the presumed site of the s-process is displayed along with the results of Winters & Macklin (1987) in Figure 1. We analyzed the $^{99}\mathrm{Tc}(n,\gamma)^{100}\mathrm{Tc}$ process using BSFM for NLD at Gogny, Brink–Axel, and Kopecky–Uhl for the γ-strength function. The present model-based evaluated findings are consistent with the data from

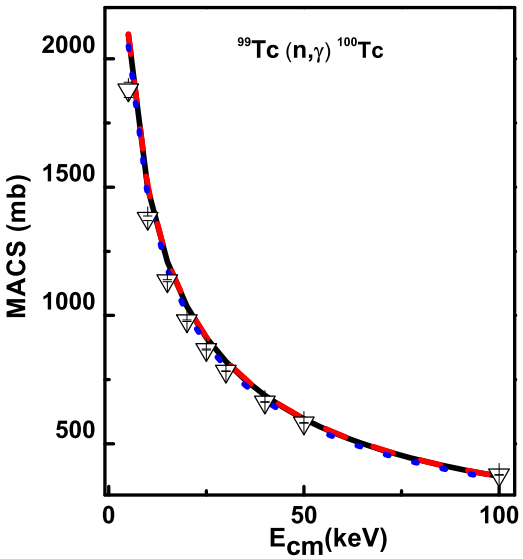

Figure 1. The MACS for ^{99}Tc(n, γ)^{100}Tc together with the measured data of Winters & Macklin (1987) (▽). The computed MACS for the ^{99}Tc(n, γ)^{100}Tc is based on the BSFM for NLD with Brink–Axel (solid line), Gogny (dashed line) and Kopecky–Uhl (dotted line) for the γ-strength function.

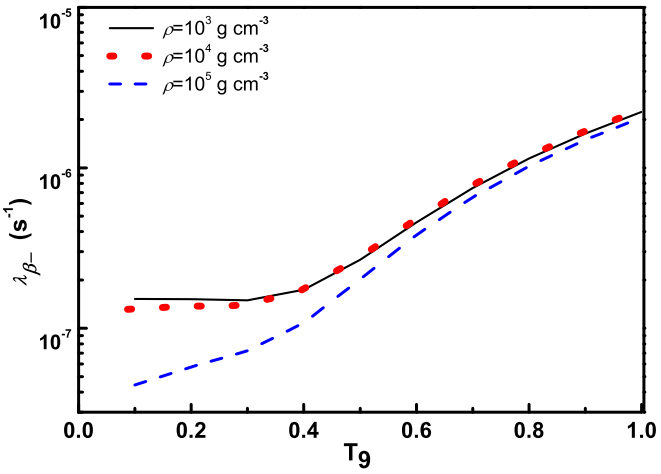

Figure 2. The temperature-dependent λ_{β^-} for ^{99}Tc at $\rho = (10^3$–$10^5)$ g cm^{-3}.

Winters & Macklin (1987), both above and below the s-process energy $kT = 30$ keV. The present analyzed MACSs at $kT = 30$ keV are 820.822 mb (Brink–Axel for γ-strength function), 822.694 mb (Gogny for γ-strength function), and 797.613 mb (Kopecky–Uhl for γ-strength function). Employing Brink–Axel, Gogny, and Kopecky–Uhl for the γ-strength function, the percentage differences between the present analysis and that of Winters & Macklin (1987) are 4.83%, 4.82%, and 1.83%, respectively. Our computed MACSs are within the range of $(5 < kT < 80)$ keV, which is consistent with the results of Macklin (1982).

In the present investigation, ^{99}Tc indicates the stable isotope of Tc in the terrestrial environment. However, the temperatures in the stellar conditions are high enough that the excited states of parent nuclei are most likely occupied. A substantial contribution to the total stellar rates comes from each excited state. Consequently, all partial decay rates attributable to each parent excited state must be taken into consideration using the microscopic rate analysis approach. We employed the pn-QRPA approach to accomplish this objective. The pn-QRPA Hamiltonian (Equation (9)) includes Nilsson-deformed potential and residual interaction components. Our investigation utilizes β_2 as an input parameter adopted from the finite range droplet macroscopic model (FRDM) and the folded Yukawa single-particle microscopic model (Möller et al. 2016). In the FRDM calculations, an improved treatment of deformation was undertaken. The model incorporated an additional macroscopic model parameter (density-symmetry coefficient) allowing a better treatment for deformed nuclei. The authors tabulated the atomic mass excesses and binding energies, ground-state shell-plus-pairing corrections, ground-state microscopic corrections, and nuclear ground-state deformations of 9318 nuclei ranging from $A = 16$ to 339. The error of the mass model was 0.5595 MeV for the entire region of nuclei included in the adjustment. The residual interaction χ and κ parameters have been optimized according to the percentage difference between the experimental half-life and the present predicted half-life of the ^{99}Tc nucleus, which is 1.48% in the present investigation. We present β^- rates (λ_{β^-}) for ^{99}Tc across various stellar temperatures and densities. The λ_{β^-} are computed at $\rho = (10^3$–$10^5)$ g cm^{-3}, $T_9 = (0.1$–$1.0)$ and are depicted in Figure 2. We note that at different densities, the λ_{β^-} increases with the stellar temperature. It is clear from Figure 2 that, at $\rho = 10^5$ g cm^{-3}, the λ_{β^-} is lower by an order of magnitude than the λ_{β^-} at $\rho = 10^3$ g cm^{-3}. However, at higher temperature, the λ_{β^-} is approximately the same as depicted in Figure 2. At $\rho = (10^3$–$10^4)$ g cm^{-3} the λ_{β^-} is almost constant with the factor of 10^{-7}. The λ_{β^-}, as indicated by the dashed line in Figure 2, does, however, exhibit a significant variation at $\rho = 10^5$ g cm^{-3}.

Furthermore, we have computed the $\lambda_{(n,\gamma)}$ by employing Equation (20). For the present purposes, we take into account $\rho X_4 = 2000$ g cm^{-3} (at $\rho = 10^4$ g cm^{-3} and $X_4 = 0.2$). σ_{22} represents the best-fit cross-section for the ^{22}Ne(n, γ)^{23}Ne process, based on TALYS v1.96, $\sigma_{22} = 0.498$ mb which is within the range of measured cross-section $\sigma_{22} = 0.9 \pm 0.7$ mb of Almeida & Kappeler (1983). The neutron captures rates are computed to be larger on $\sigma_i = 797.613$ mb at the s-process energy ($kT = 30$ keV) for ^{99}Tc. At this cross-section the $\lambda_{(n,\gamma)}$ is plotted with λ_{β^-} as depicted in Figure 3. One can see that the thermal neutron capture rates are larger than those of temperature-dependent β^- decay rates. The $\lambda_{(n,\gamma)}$ and λ_{β^-} are crossing each other at $T_9 = 0.26$. The $\lambda_{(n,\gamma)}$ is higher than λ_{β^-} at high temperature (Figure 3 provides more detailed descriptions). This is due to the fact that at $T_9 > 0.26$, neutron

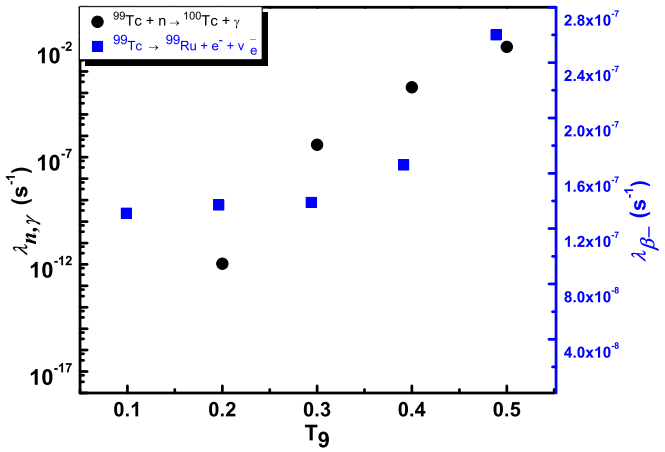

Figure 3. The temperature-dependent $\lambda_{(n,\gamma)}$ (solid circles) and λ_{β^-} (solid rectangles) for ^{99}Tc at $\rho = 10^4$ g cm^{-3}.

emission rates are rising. At lower temperatures, the neutron density is not feasible for the *s*-processes. Thus, at lower temperatures, λ_{β^-} is larger than $\lambda_{(n,\gamma)}$.

4. Conclusion

Let us simply outline the key results and draw conclusions from them.

1. Across a wide range of energies, we have examined the MACS of the (n,γ) process for ^{99}Tc within the framework of TALYS v1.96. Employing multiple γ-strength function models from TALYS, the MACS has been generated for the ^{99}Tc$(n,\gamma)^{100}$Tc radiative capture process. The calculated values were compared to the measurements of previous studies. We found that, out of all the γ-strength function models, the Brink–Axel of TALYS fits for the ^{99}Tc$(n,\gamma)^{100}$Tc radiative capture process is the best. The provided experimental data can be precisely generated by the H-B theory prediction with all of the parameter and model adjustments.
2. We computed the stellar rates for ^{99}Tc in the context of the pn-QRPA for a wide range of stellar temperatures and densities. The pn-QRPA theory effectively calculates weak interaction rates (λ_{β^-}) for ^{99}Tc. We noted that at low densities the λ_{β^-} are higher by an order of magnitude than the λ_{β^-} at higher densities, as one can see from Figure 2.
3. In the third part of our study, we compared $\lambda_{(n,\gamma)}$ and λ_{β^-} under similar stellar scenarios. It was observed that, at $T_9 = 0.26$, the stellar β^- decay rates are almost equal to the neutron capture rates. Beyond this temperature, the neutron capture rates surpass the β^- decay rates.

Acknowledgments

J.-U.N. would like to acknowledge the financial support of the Higher Education Commission Pakistan through project number 20-15394/NRPU/R&D/HEC/2021.

Declaration of Competing Interest

The authors declare that they have no known competing financial interests or personal relationships that could have appeared to influence the work reported in this paper.

References

Almeida, J., & Kappeler, F. 1983, ApJ, 265, 417
Baade, W., & Zwicky, F. 1934, PNAS, 20, 254
Bethe, H.A. 1939, PhRv, 55, 434
Bisterzo, S., Gallino, R., Kppeler, F., et al. 2015, MNRAS, 449, 506
Brink, D.M. 1957, NucPh, 4, 215
Burbidge, E. M., Burbidge, G. M., Fowler, W. A., & Hoyle, F. 1957, RvMP, 29, 547
Busso, M., Gallino, R., Lambert, L.D., Travaglio, C., & Smith, V.V. 2001, ApJ, 557, 802
Cameron, A. G. W. 1959, ApJ, 130, 452
Dilg, W., Schantl, W., Vonach, H., & Uhl, M. 1973, NuPhA, 217, 269
Goriely, S., Hilaire, S., Pru, S., & Sieja, K. 2018, PhRvC, 98, 014327
Harada, H., Nakamura, S., Katoh, T., & Ogata, Y. 1995, JNST, 32, 395
Hardy, J. C., & Towner, I. S. 2009, PhRvC, 79, 055502
Hauser, W., & Feshbach, H. 1952, PhRv, 87, 366
Hektor, A., Kolbe, E., Langanke, K., & Toivanen, J. 2000, PhRvC, 61, 055803
Hirsch, M., Staudt, A., & Klapdor-Kleingrothaus, H. V. 1992, ADNDT, 51, 243
Hirsch, M., Staudt, A., Muto, K., & Klapdorkleingrothaus, H. V. 1993, ADNDT, 53, 165
Homma, H., Bender, E., Hirsch, M., et al. 1996, PhRvC, 54, 2972
Iben, I., & Truran, J. W. 1978, ApJ, 220, 980
Kabir, A., Nabi, J. U., Tahir, M., Muneem, A., & Abideen, Z. U. 2024, ChPhC, 48, 094101
Klapdor-Kleingrothaus, H.V., Metzinger, J., & Oda, T. 1984, ADNDT, 31, 81
Kondev, F. G., Wang, M., Huang, W. J., Naimi, S., & Audi, G. 2020, ChPhC, 45, 030001
Koning, A.J., & Delaroche, J.P. 2003, NuPhA, 713, 231
Koning, A.J., Hilaire, S., & Goriely, S. 2008, NuPhA, 810, 13
Koning, A. J., Hilaire, S., & Goriely, S. 2021, TALYS—1.96 A Nuclear Reaction Program, User Manual (Netherlands: Nuclear Research and Consultancy Group (NRG))
Kopecky, J., & Ulh, M. 1990, PhRvC, 41, 1941
Lugaro, M., Herwig, F., Lattanzio, J. C., Gallino, R., & Straniero, O. 2003, ApJ, 586, 1305
Macklin, R. L. 1982, NSE, 81, 520
Mathews, G. J., Takahashi, K., Ward, R. A., & Howard, W. M. 1986, ApJ, 302, 410
Möller, P., & Randrup, J. 1990, NuPhA, 514, 1
Möller, P., Sierk, A. J., Ichikawa, T., & Sagawa, H. 2016, ADNDT, 1, 109
Muto, K., Bender, E., Oda, T., & Klapdor-Kleingrothaus, H.V. 1992, ZPhyA, 341, 407
Nabi, J.-U., & Klapdor-Kleingrothaus, H.V. 1999, ADNDT, 71, 149
Nabi, J.-U., & Klapdor-Kleingrothaus, H.V. 2004, ADNDT, 88, 237
Ragnarsson, I., & Sheline, R.K. 1984, PhyS, 29, 385
Shetye, S., Van Eck, S., Goriely, S., et al. 2020, A&A, 635, 6
Shetye, S., Van Eck, S., Jorissen, A., et al. 2021, A&A, 650, 118
Staudt, A., Bender, E., Muto, K., & Klapdor-Kleingrothaus, H. V. 1990, ADNDT, 44, 79
Usman, S., & Mushtaq, A. 2023, NatSR, 13, 15315
Winters, R. R., & Macklin, R. L. 1987, ApJ, 313, 808